Direct visualization of the impurity occupancy roadmap in Ni-substituted van der Waals ferromagnet Fe3GaTe2

Journal:	*Nano Letters*
Manuscript ID	nl-2024-058112.R2
Manuscript Type:	Communication
Date Submitted by the Author:	n/a
Complete List of Authors:	Yuan, Jian; ShanghaiTech University Wang, Haonan; East China Normal University, Department of Electronics Hou, Xiaofei; ShanghaiTech University Zhang, Binshuo; ShanghaiTech University, School of Physical Science and Technology Wei, Yurui; ShanghaiTech University, School of Information Science and Technology Guo, Jiangteng; Nankai University, School of Physics Sun, Lu; ShanghaiTech University Yu, Zhenhai; ShanghaiTech University, School of Physical Science and Technology Liu, Xiangqi; ShanghaiTech University, Xia, Wei; ShanghaiTech University, School of Physical Science and Technology Wang, Xia; ShanghaiTech University, School of Physical Science and Technology Liu, Xuerong; ShanghaiTech University, School of Physical Science and Technology Chen, Yulin; ShanghaiTech University Zhang, Shihao; Hunan University Fu, Xuewen; Nankai University, Physics Qu, Ke; East China Normal University Yang, Zhenzhong; East China Normal University, Guo, Yanfeng; ShanghaiTech University, School of Physical Science and Technology

Direct visualization of the impurity occupancy roadmap in Ni-substituted van der Waals ferromagnet Fe_3GaTe_2

Jian Yuan[1†], Haonan Wang[2†], Xiaofei Hou[1†], Binshuo Zhang[1†], Yurui Wei[3], Jiangteng Guo[4], Lu Sun[3], Zhenhai Yu[1], Xiangqi Liu[1], Wei Xia[1,7], Xia Wang[1,6], Xuerong Liu[1], Yulin Chen[1,8], Shihao Zhang[5]*, Xuewen Fu[4]*, Ke Qu[2]*, Zhenzhong Yang[2], Yanfeng Guo[1,7]*

[1]*School of Physical Science and Technology, ShanghaiTech University, Shanghai 201210, China*

[2]*Key Laboratory of Polar Materials and Devices (MOE), Ministry of Education, Shanghai Center of Brain-inspired Intelligent Materials and Devices, Department of Electronics, East China Normal University, Shanghai 200241, China*

[3]*School of Information Science and Technology, ShanghaiTech University, Shanghai 201210, China*

[4]*Ultrafast Electron Microscopy Laboratory, Key Laboratory of Weak-Light Nonlinear Photonics (Ministry of Education), School of Physics, Nankai University, Tianjin 300071, China*

[5]*School of Physics and Electronics, Hunan University, Changsha 410082, China*

[6]*Analytical Instrumentation Center, School of Physical Science and Technology, ShanghaiTech University, Shanghai 201210, China*

[7]*ShanghaiTech Laboratory for Topological Physics, ShanghaiTech University, Shanghai 201210, China*

[8]*Clarendon Laboratory, Department of Physics, University of Oxford, Oxford OX1 3PU, United Kingdom*

ABSTRACT

Impurity substitution is effective to study the intrinsic properties of a quantum material. When the target element has multiple Wyckoff positions, it is challenging but essential to know the exact position and occupancy order of impurity atoms. Via comprehensive experimental and theoretical investigations, we establish the Ni substitution roadmap in the van der Waals ferromagnet Fe_3GaTe_2. The results unambiguously reveal that in $(Fe_{1-x}Ni_x)_3GaTe_2$, Ni atoms initially form interlayer gap Ni3 sites when $x < 0.1$, and then gradually occupy Fe2 sites. When $x > 0.75$, they start to substitute for Fe1 sites and eventually realize full occupation. Accordingly, T_C and saturation moments both show nonlinear decrease tied to different roles of Ni3, Fe1 and Fe2 sites in the spin Hamiltonian. The results not only yield fruitful insights into the roles of different Fe sites in Fe_3GaTe_2, but also set a paradigm for future impurity substitution study on other quantum materials.

Key Words: *van der Waals ferromagnet, high Curie temperature, impurity substitution, magnetic exchange*

Impurity substitution in a solid can serve as an effective way to probe the mechanism underlying the physical properties. This strategy has played crucial roles in understanding the pairing symmetry of various superconductors. According to the Anderson's theorem,[1] nonmagnetic impurity substitution in a superconductor with an isotropic superconducting gap influences the Cooper pairs negligibly, but can break them in a superconductor with an anisotropic gap. As a sharp contrast, magnetic impurities can cause pair-breaking effect regardless of the gap type. Guided by this theory, the Zn^{2+} with a tightly closed *d* shell was widely used as an ideal impurity to study the pairing mechanisms of both cuprate and iron-based superconductors.[2–13] Besides, the impurity substitution was also used as an approach to investigate the origin of many-body interactions in cuprate superconductors, because the substitution effect on the low-energy dynamics could be viewed as a magnetic analogue of the isotope effect.[14]

The impurity substitution strategy is also widely adopted to study the recently emerged van der Waals (vdW) magnets Fe_nGeTe_2 (n = 3, 4, 5) and Fe_3GaTe_2.[15–21] The inherent magnetocrystalline anisotropy in the vdW magnets stabilizes the magnetic order against finite temperature, thus violating the Merin-Wagner theorem and realizing long-range magnetic order in a broad range of vdW magnets in mono- or few-layer form, such as in CrI_3, $Cr_2Ge_2Te_6$, $Cr_2Si_2Te_6$, VSe_2, and $MnSe_2$,[22–27] etc. The itinerant ferromagnets Fe_nGeTe_2 (n = 3, 4, 5) are characterized by the remarkably high Curie temperature T_C and therefore have been subjected to intensively investigations.[28–31] Interestingly, the T_C of Fe_nGeTe_2 is tunable by controlling the Fe content,[32–34] suggesting the pivotal role of Fe in the magnetic exchange. However, the multiple Fe Wyckoff sites in the lattice of Fe_nGeTe_2 give rise to complicated magnetic orders, which makes the understanding about the spin Hamiltonian extremely difficult. In Fe_3GeTe_2 and Fe_5GeTe_2, the substitution of Ni and Co shows distinct behaviors, where Co and Ni substitutions in Fe_3GeTe_2 gradually suppress the ferromagnetic (FM) order, while Ni substitution in Fe_5GeTe_2 significantly enhances the T_C even up to ~ 480 K and Co substitution results in an antiferromagnetic (AFM) state.[15–20,35–37] However, with these substitutions, it remains unknown that whether the impurities enter onto the Fe sites or not, and what is the order for impurities to occupy the different Fe sites, thus hindering a direct understanding about the delicate roles of the impurities and the different Fe sites in the complex magnetic exchanges.

The recently emerged Fe_3GaTe_2, which is isostructural with Fe_3GeTe_2, has a very high T_C of ~ 380 K.[38] In the centrosymmetric crystal structure, the Dzyaloshinskii-Moriya interaction (DMI) caused by the introduction of Fe deficiency and hence the spatial inversion symmetry breaking, rather than the competition between magnetic dipole interaction and strong perpendicular uniaxial anisotropy, is suggested as the driven force for the observed room-temperature Néel-type skyrmions.[39,40] Regarding the intriguing magnetic properties related to the Fe sites, impurity substitution would yield valuable insights. A very recent impurity study work unveiled that a small amount of Co or Ni substitution in Fe_3GaTe_2 results in T_C suppression. Specifically, the Co substitution turns the FM state into an AFM one and then to the spin-glass state, while Ni substitution turns the magnetic states from the FM state into the spin-glass state.[21] To fully understand these effects and establish the spin Hamiltonian for impurity substitution, precisely tracing the roadmap for impurity occupation in the crystal lattice is very necessary.

In this work, by employing first-principles calculations, Cs-corrected scanning transmission electron microscopy (STEM), Lorentz transmission electron microscopy (L-TEM), magneto-optical Kerr effect (MOKE) microscopy and magnetization measurements, we established a clear roadmap for the Ni occupancy in $(Fe_{1-x}Ni_x)_3GaTe_2$ with x up to 1.0.

As is schematically drawn in Figure 1a, Fe_3GaTe_2 crystallizes into a hexagonal structure (space group: $P6_3$/mmc) with the lattice parameters $a = b = 3.9860$ Å, $c = 16.2290$ Å, $\alpha = \beta = 90°$, and $\gamma = 120°$. In this structure, the vdW gap is between two adjacent Te atoms, and there are two Fe Wyckoff positions in each layer of the lattice, which we refer to as Fe1 and Fe2. The slabs of Fe_3GaTe_2 are stacked along the c-axis with the interlayer space of ~ 0.78 nm. Our first-principles calculations indicate that on Fe1 and Fe2 sites the magnetic moments are 1.33 μ_B/Fe1 and 1.98 μ_B/Fe2, respectively. In this layered structure, the intralayer exchange between the nearest Fe2 along out-of-plane direction is 26.0 meV, which is the main contribution to the FM order.

As a comparison, in the crystal structure of Ni_3GaTe_2 as shown in Figure 1b, there are additional Ni3 Wyckoff sites locating in the vdW gap. The different Fe and Ni Wyckoff sites in the two compounds make the occupancy of Ni in Fe_3GaTe_2 very confusing. The Bragg reflection index on the XRD spectrum of $(Fe_{1-x}Ni_x)_3GaTe_2$ ($x = 0 – 1.0$) crystals confirms the (00l) orientation, and no impurity peaks were detected within the instrument resolution limit, as shown in Figure S1 of the Supplementary Information (SI). The peaks of XRD for each composition can be satisfactorily indexed on basis of the hexagonal structure with the space group $P6_3$/mmc, suggesting the phase purity of our specimens. As illustrated in Figure 1c, the main peaks of all compositions exhibit a continuous shift to higher angle with Ni substitution till $x = 0.7$, unveiling a monotonic decrease of the c-axis with increase of Ni. When $x > 0.7$, the change of c shows almost saturation. The derived values of c-axis from the PXRD data analysis are summarized in Table S1 of SI. The compositions were measured by using energy dispersive X-ray spectroscopy (EDS), with the results shown in Figure S2 and Table S2 of SI. We thereafter use the measured substitution concentration for each sample.

Figure 1d shows the temperature dependent magnetization curves $M(T)$ for $(Fe_{1-x}Ni_x)_3GaTe_2$, which exhibits typical FM order with a T_C at ~ 350 K, where T_C is determined by the peak of $dM(T)/dT$. With the increase of x, T_C is gradually suppressed, which can be clearly seen in Figure 1f. When $x = 0.28$, T_C decreases to ~ 50 K, while when the substitution is gradually increased up to $x = 1.0$, the FM order completely disappears, which is consistent with the fact that Ni_3GaTe_2 is essentially nonmagnetic.[41] The evolution of isothermal magnetization $M(H)$ at 2 K for various x is consistent with the $M(T)$, clearly displaying the suppression of ferromagnetism, as seen in Figure 1e. In Figure 1f, the nonlinear evolution of T_C and saturation magnetization M_S follows the same trend with x, which shows that the decrease of T_C is initially very fast from 350 K to ~ 100 K before $x = 0.1$ and then is somewhat moderate till it is invisible. Considering this nonlinear evolution of T_C and M_S with x and the fact that Ni_3GaTe_2 has three Ni sites, it is crucial to trace the positions of substituted Ni and study its effect on the magnetism. Furthermore, homogeneity and stability of the dopants are also necessary to be investigated.

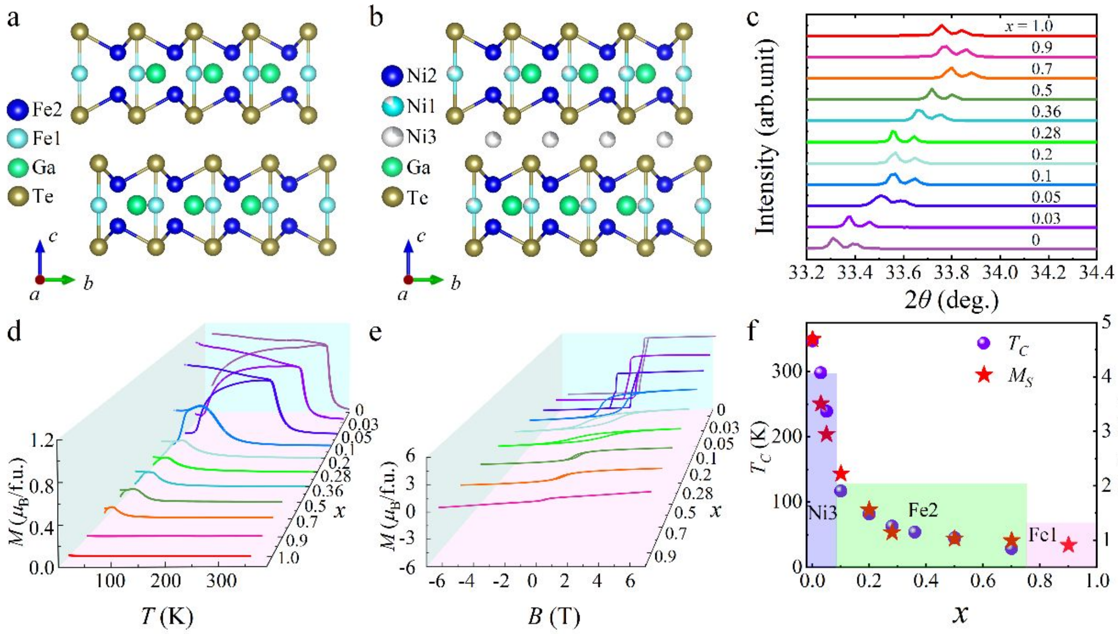

Figure 1. Crystal structure and magnetizations of $(Fe_{1-x}Ni_x)_3GaTe_2$. (a)-(b) Schematic views of the crystal structure of Fe_3GaTe_2 and Ni_3GaTe_2 along the *a*-axis, respectively. (c) The PXRD of the (00l) orientation of $(Fe_{1-x}Ni_x)_3GaTe_2$. (d) Temperature dependent magnetizations of $(Fe_{1-x}Ni_x)_3GaTe_2$ ($x = 0 – 1.0$) under a 0.1 T magnetic field which is perpendicular to the *ab*-plane. (e) Out-of-plane isothermal magnetizations at 2 K. (f) The evolution of T_C and M_S at 2 K against x. The height and width of the rectangles represent the moment size and x to achieve a full occupancy on each site, respectively.

Aberration-corrected high-angle annular-dark-field (HAADF) STEM and annular bright-field (ABF) STEM are used to obtain atomic-resolution images of Ni-substituted Fe_3GaTe_2. The image intensity in HAADF-STEM mode of an atomic column is approximately proportional to the atomic number to the power of $1.7/Z^{1.7}$, that is, brighter spots in the images are indicative of heavier atoms in the region or similarly a greater atomic density. ABF-STEM images collect scattered electrons in a lower angle range, which can simultaneously image both light and heavy atomic species and are more sensitive to less atomic density. On the contrary to the contrast of HAADF-STEM image, dark spots are indicative of the presence of atoms in ABF-STEM mode. Therefore, by combining HAADF-STEM and ABF-STEM imaging, we can map out of the occupancy of Ni dopants within the Ni-substituted Fe_3GaTe_2 at the atomic level.

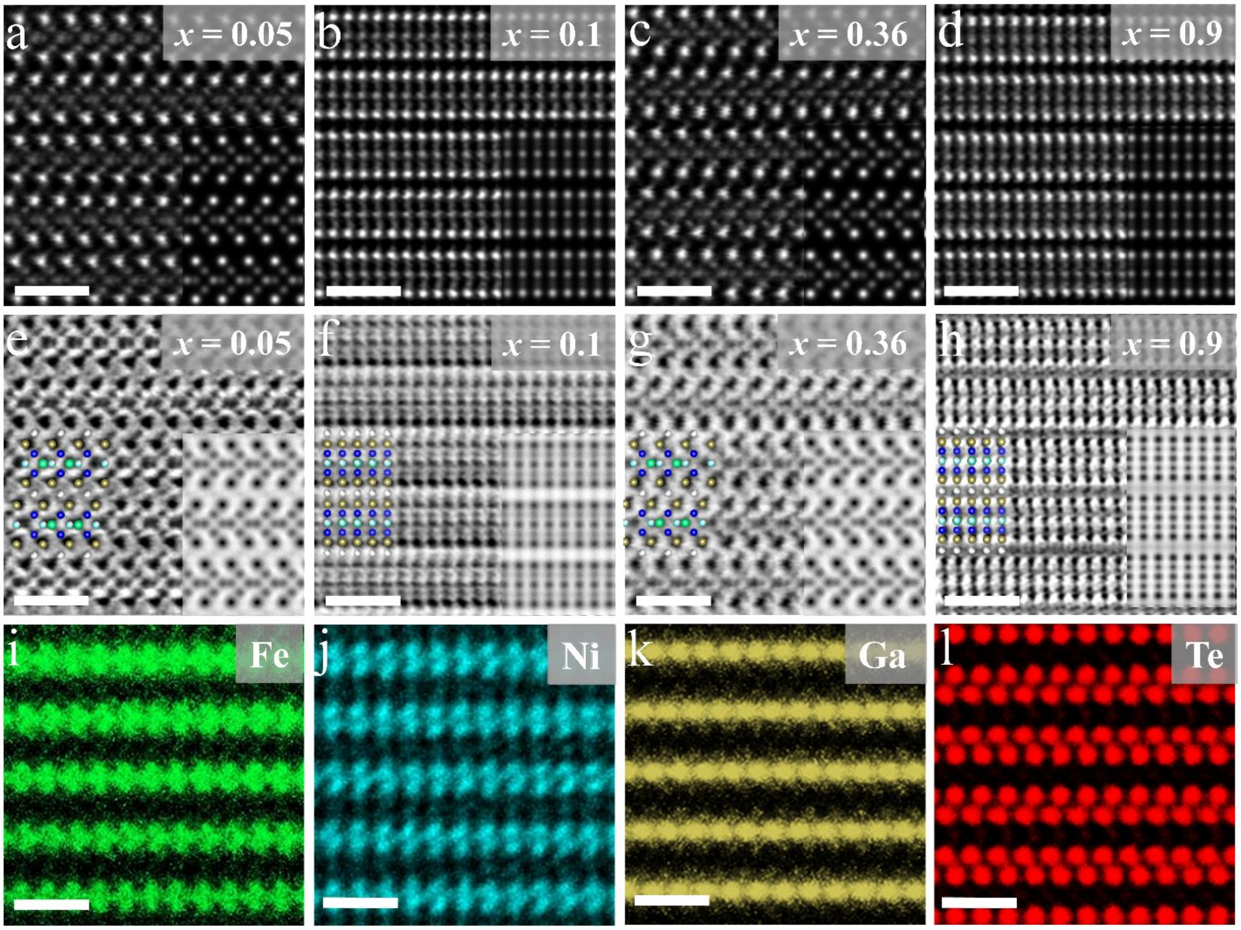

Figure 2. STEM images of $(Fe_{1-x}Ni_x)_3GaTe_2$ crystals with EDS mappings of Fe, Ni, Ga and Te atoms viewed along the [100] ($x = 0.05$ and $x = 0.36$) and [120] ($x = 0.1$ and $x = 0.9$) zone axes. The HAADF-STEM images in (a)-(d) for $x = 0.05$, 0.1, 0.36 and 0.9 and the corresponding ABF-STEM images are in (e)-(h), respectively. Simulated images are overlaid on the HAADF and ABF-STEM images. In (e)-(h), the cyan, blue, green, and brown balls in the crystal models represent Fe1, Fe2, Ga, and Te atoms, respectively. (i)-(l) EDS mappings of $(Fe_{0.64}Ni_{0.36})_3GaTe_2$. The scale bars in the images are 1 nm.

Figures 2a-2d and Figures 2e-2f show the atomic-resolution HAADF and ABF-STEM images of $(Fe_{1-x}Ni_x)_3GaTe_2$, when $x = 0.05$, 0.1, 0.36, and 0.9 respectively. Simulated HAADF/ABF-STEM images are shown as insets in the lower right corner of each figure, which are consistent with experimental images. The results demonstrate that initially, substituted Ni atoms preferentially occupy the interlayer Ni3 sites (Figures 2a-2h). This is unsurprising, because Ni_3GaTe_2 possesses three distinct Ni occupation sites, unlike Fe_3GaTe_2 with only two Fe sites. Notably, the vdW gap between layers is partially filled with Ni atoms (0.25 occupancy), while the Ni1 site has a 75% occupancy.[41] EDS mapping results for $x = 0.36$ (Figures 2i-2l) reveal the formation of Ni3 sites. Subsequently, additional Ni atoms preferentially occupy the intralayer Fe2 sites, as shown in the EDS mapping results for $x = 0.36$ (Figures 2i-2l). Comparing the distribution of Fe and Ni atoms at $x = 0.36$, it is evident that Fe atoms remain in both Fe1 and Fe2 sites, while Ni atoms are restricted to Ni3 and Fe2 sites. This result is further supported by the plotted intensity of Fe and Ni atoms with their distribution in Figure S3. This demonstrates that Ni atoms would actually occupy the Fe2 sites after they fill the Ni3 sites. It is quite different from the Ni atoms in $(Fe_{1-x}Ni_x)_5GeTe_2$ at $x = 0.36$, which lead to the coexistence of flat and rumpled atomic planes due to Fe-rich and Ni-rich atoms, respectively, rather than occupy different Fe sites in a special order.[37] Furthermore, with increasing Ni substitution levels, Ni atoms progressively occupy the Fe1 sites, eventually achieving complete occupancy at $x = 1.0$.

The detailed isothermal magnetizations of $(Fe_{1-x}Ni_x)_3GaTe_2$ at various temperatures measured with the magnetic field perpendicular to the *ab*-plane are presented in Figure 3, which clearly show the evolution of ferromagnetism with both temperature and Ni substitution level. When $x = 0$, the hysteresis loop signifying the ferromagnetism is even visible above 300 K, which is consistent with the fact that the T_C is of about 350 K. As x increases, the hysteresis loop becomes wider accompanied by larger saturation magnetic field and smaller saturation moment. While when $x = 0.1$, the hysteresis loop changes from square to circular shape, which then becomes narrower as x is further increased. The evolution of hysteresis loop is fully consistent with the STEM results, that is, when the x is smaller ($x < 0.1$), Ni atoms enter onto the interlayer Ni3 sites, resulting in a sudden drop of the T_C and saturation moment while a quick increase of the coercive field, seen in Figure 1f, while the hysteresis loop remains a rectangular shape signifying the ferromagnetism, suggesting that the substituted crystals are pinning-type ferromagnets and the motion of domain wall becomes difficult. When $x > 0.1$, Ni substitutions start to occupy the Fe2 and then the Fe1 sites and the magnetic hysteresis loops are no longer rectangular.

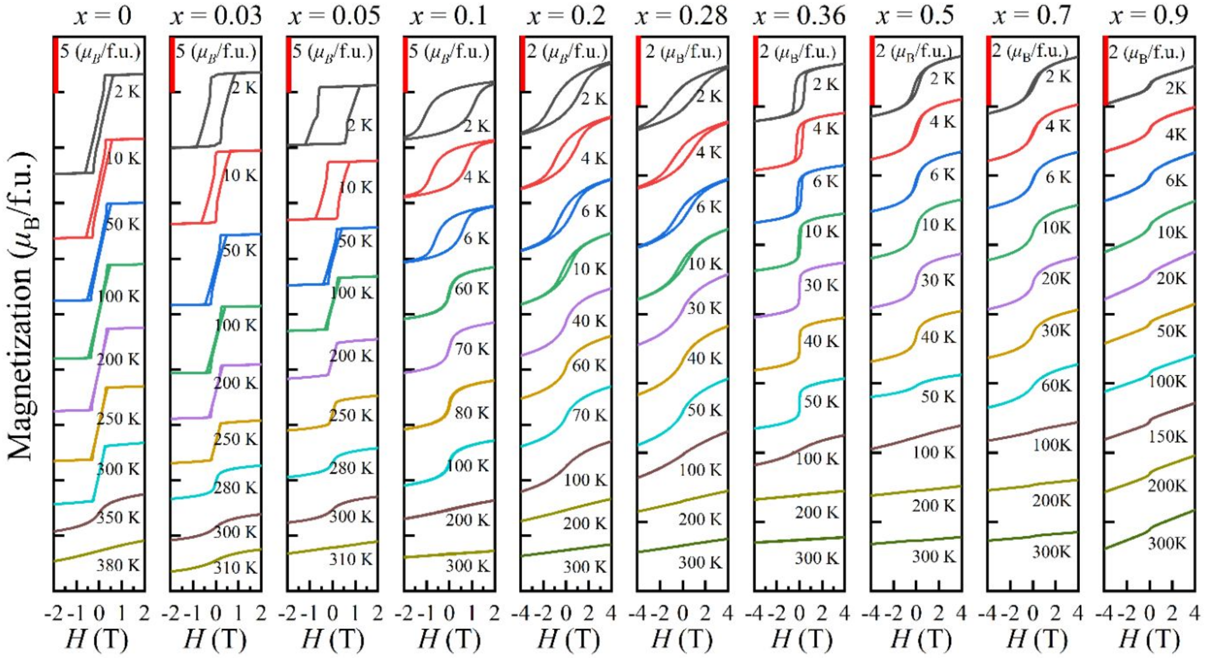

Figure 3. Ni substitution level *x* and temperature dependence of isothermal magnetizations measured with the magnetic field perpendicular to the *ab*-plane.

First-principles calculations can yield in-depth insights into the Ni substitution effect on the magnetism. Since the vdW interlayer gap is filled with 0.25 Ni atoms, which suggests a maximum x of about 0.083 (1/12) for that the occupancy of Ni3 site reaches 0.25 in $(Fe_{1-x}Ni_x)_3GaTe_2$, so a supercell with 24 Fe sites (2 × 2 × 1 supercell) was used in the calculations. The calculated electronic bands of $(Fe_{1-x}Ni_x)_3GaTe_2$ with $x = 0$, 1/24, 1/12, and 3/24 are presented in Figures 4a-4d. It is apparent that the Ni substitution makes the energy bands less dispersive, and the impurity bands reduce the itinerant magnetism. During Ni substitution, the resulting Fe vacancies generate local magnetism, thereby boosting the correlation effect. Thus, $(Fe_{1-x}Ni_x)_3GaTe_2$ hold both local magnetism and itinerant magnetism due to the Fe vacancies caused by Ni doping. In the first step with the Ni substitution, i.e., when the Ni forms the interlayer Ni3 sites, the magnetic moment decreases about 4.1 μ_B per Ni atom, which indicates that substituted Ni atoms strongly weaken the itinerant magnetism. When Ni3 occupancy is larger than 0.25 ($x = 3/24$), there are three Ni atoms and three Fe vacancies in the supercell model and 9 cases with lowest energies are plotted in Figure

S4 and their energies are listed in the Table S3. The total energy of Fe2 is lower than that of Ni3 by 0.52 eV per Ni atom and lower than that of Fe1 by 0.41 eV per Ni atom. Thus, the substituted Ni atoms prefer to occupy the Fe2 site in the second step. During this process, the magnetic moment decreases 2.5 μ_B per Ni atom. It indicates somewhat moderate suppression of the FM as compared to that in the first step, because the (Fe/Ni)2 site still keeps the conducting channels for itinerant electrons. This is fully consistent with our magnetization measurements. Moreover, the Fe vacancy has significant effect on the FM exchange. When $x = 1/24$, as shown in Figure 4e, assuming that in the layer without Fe vacancy, the substituted Ni atoms reduce the FM exchange interaction between the Fe2 sites near the Ni atom from 26 meV [42–44] to 17.9 meV. When the layer is with Fe vacancy, the Fe vacancy remarkably influences the exchange interactions among other magnetic sites. For example, the exchange integral between Fe1 and Fe2 near the vacancy is increased to 13.1~20.8 meV, which are much larger than that of pristine Fe_3GaTe_2 (8.8 meV). The exchange interaction parameters are plotted in Figure S5. Thus, the Fe vacancies and Ni dopants simultaneously result in the inhomogeneity in $(Fe_{23/24}Ni_{1/24})_3GaTe_2$ and obviously affect the magnetic exchanges.

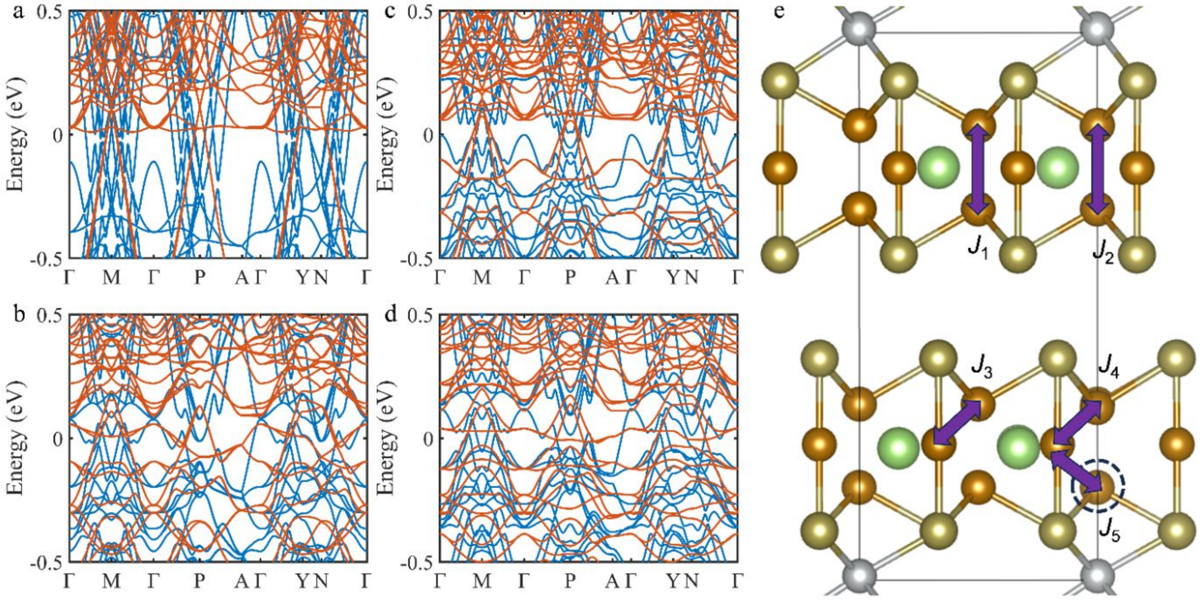

Figure 4. The calculated band structures of $(Fe_{1-x}Ni_x)_3GaTe_2$. (a)-(d) The energy bands of $(Fe_{1-x}Ni_x)_3GaTe_2$ (x = 0, 1/24, 1/12, 3/24). The blue and red lines refer to the spin-up and spin-down energy bands, respectively. (e) The structure of $(Fe_{23/24}Ni_{1/24})_3GaTe_2$. Here the black dashed circle refers to the Fe vacancy. The different exchange parameters J_1~J_5 are shown in the figure, where J_1 = 26.9 meV, J_2 = 17.9 meV, J_3 = 13.1 meV, J_4 = 18.8 meV and J_5 = 20.8 meV. The positive values of J_1~J_5 represent the FM exchanges.

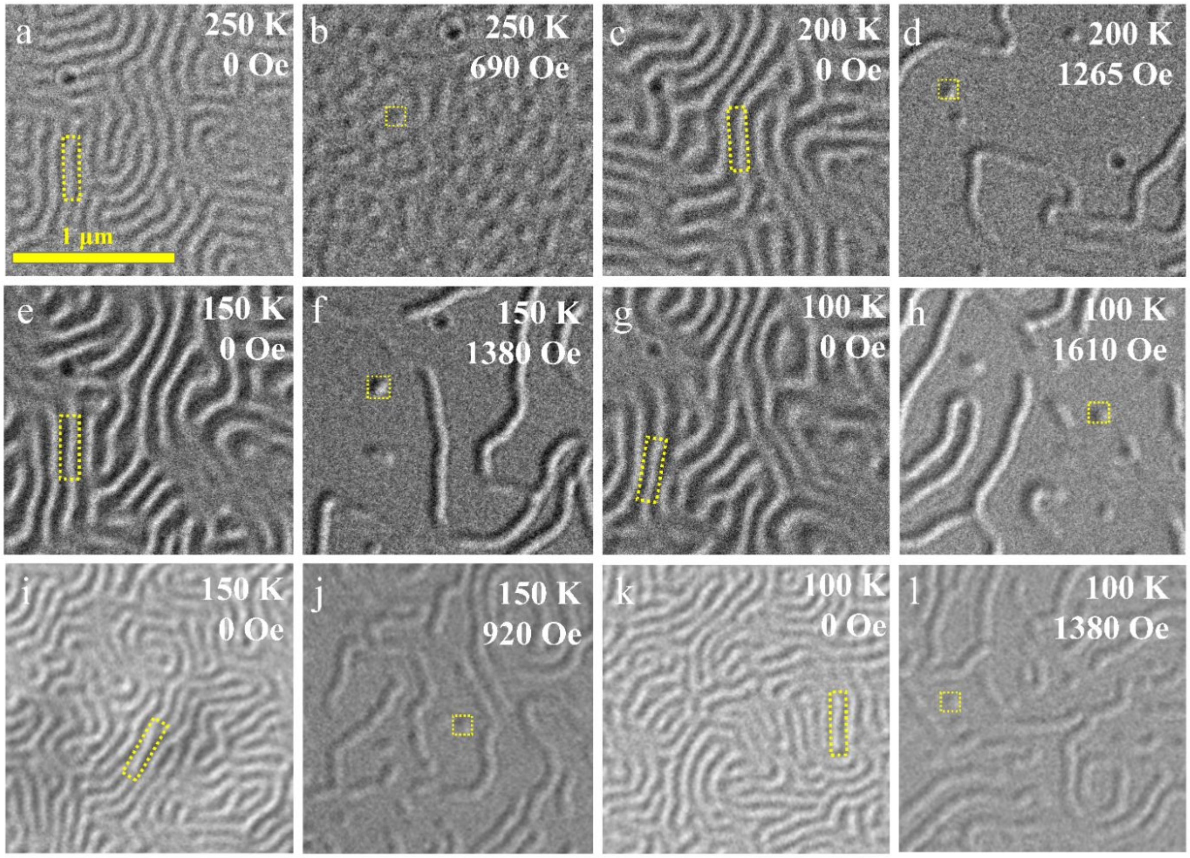

Figure 5. L-TEM results for $(Fe_{0.97}Ni_{0.03})_3GaTe_2$ and $(Fe_{0.95}Ni_{0.05})_3GaTe_2$ flakes. (a)-(h) Labyrinth domain structures and magnetic skyrmions in $(Fe_{0.97}Ni_{0.03})_3GaTe_2$ with different temperatures. (i)-(l) Labyrinth domain structures and magnetic skyrmions in $(Fe_{0.95}Ni_{0.05})_3GaTe_2$ with different temperatures. The surface is within the *ab*-plane with the magnetic field perpendicular to the surface. The images are taken at α = 15° and d = -3 mm, where α is the angle between the sample surface and the x - y plane, d is the focus distance with the positive value representing the over-focus and negative value denoting the under-focus.

To study more details about the drastic suppression of FM in $(Fe_{1-x}Ni_x)_3GaTe_2$ when $x < 0.1$, we selected two representative specimens, $x = 0.03$ and $x = 0.05$, in which the saturation moments are significantly reduced, to measure their magnetic domain structures by using L-TEM. As is presented in Figures 5a-5h, the measurements on a $(Fe_{0.97}Ni_{0.03})_3GaTe_2$ flake unveil clear labyrinthine domain structures at different temperatures below 300 K with large patterns and wide walls, indicating the presence of strong ferromagnetism. As the temperature increases, the width of domain walls gradually becomes narrower. When a magnetic field perpendicular to the *ab*-plane is applied during the measurements, the labyrinthine magnetic domains of $(Fe_{0.97}Ni_{0.03})_3GaTe_2$ gradually transform into skyrmion spin textures when the magnetic field is sufficiently large to polarize the sample, i.e. above 1600 Oe, as seen in Figures 5i-5l. Magnetic skyrmions of $(Fe_{1-x}Ni_x)_3GaTe_2$ are observed under the magnetic fields of 1610 Oe, 1380 Oe, 1265 Oe, and 690 Oe at 100 K, 150 K, 200 K, and 250 K, respectively. At 100 K, $(Fe_{0.97}Ni_{0.03})_3GaTe_2$ and $(Fe_{0.95}Ni_{0.05})_3GaTe_2$ both have similar labyrinthine domain structures and skyrmions spin textures, but a close inspection unveils that the domain walls are wider and the skyrmions are larger when $x = 0.03$, as shown in Figure S8, consistent with the results of magnetization measurements. The width of domain walls can be defined as $w = 2|A/K|^{1/2}$, where A is exchange stiffness and K is uniaxial anisotropy constant.[45] The substituted Ni atoms destroy the magnetic Fe sites and decrease both the saturation magnetization M_s and total spin stiffness A. Besides, due to that the magnetic domain walls are pinned, they are hard to be moved and canceled to decrease the energy, hence the number of magnetic domains is larger. Thus, the width of domain walls is decreased with Ni substitution, and the magnetic domains will become denser as well. Meanwhile, the magnetic domain structure of bulk crystal measured by using MOKE also shows the similar evolution as observed in thin flakes, as seen in Figures S6 and S7 of SI.

To summarize, our characterizations and theoretical calculations on $(Fe_{1-x}Ni_x)_3GaTe_2$ ($x = 0$ - 1.0) crystals enable us to establish the roadmap for Ni substitution in Fe_3GaTe_2, which unveils three steps for Ni atoms to form the Ni3 sites and occupy the different Fe sites. The substitutions are accompanied by a nonlinear change of the Curie temperature and saturation magnetic moments. In the first step, Ni atoms preferentially form the interlayer Ni3 sites, which result in a fast decrease of the Curie temperature as well as the saturation magnetic moment. Subsequently, Ni atoms enter onto the Fe2 sites and then replace the Fe1 sites, resulting in the magnetic hysteresis loop change from square to circular shape and a moderate suppression of the ferromagnetism. The three-step substitution mechanism is also supported by the theoretical calculations. Since impurity substitution can also be useful method for the study of crucial issues in many quantum materials, such as the significant enhancement rather than suppression of the T_C in Ni-substituted Fe_5GeTe_2

which has three Fe sites,[20, 37] the results reported herein would provide the proof-of-principle elaboration of such study.

REFERENCES

(1) Anderson, P. W. Localized Magnetic States in Metals. *Phys. Rev.* **1961**, *124* (1), 41–53. https://doi.org/10.1103/PhysRev.124.41.

(2) Alloul, H.; Bobroff, J.; Gabay, M.; Hirschfeld, P. J. Defects in Correlated Metals and Superconductors. *Rev. Mod. Phys.* **2009**, *81* (1), 45–108. https://doi.org/10.1103/RevModPhys.81.45.

(3) Williams, G. V. M.; Tallon, J. L.; Dupree, R. NMR Study of Magnetic and Nonmagnetic Impurities in $YBa_2Cu_4O_8$. *Phys. Rev. B* **2000**, *61* (6), 4319–4325. https://doi.org/10.1103/PhysRevB.61.4319.

(4) Bernhard, C.; Niedermayer, Ch.; Blasius, T.; Williams, G. V. M.; De Renzi, R.; Bucci, C.; Tallon, J. L. Muon-Spin-Rotation Study of Zn-Induced Magnetic Moments in Cuprate High-Tc Superconductors. *Phys. Rev. B* **1998**, *58* (14), R8937–R8940. https://doi.org/10.1103/PhysRevB.58.R8937.

(5) Julien, M.-H.; Fehér, T.; Horvatić, M.; Berthier, C.; Bakharev, O. N.; Ségransan, P.; Collin, G.; Marucco, J.-F. ^{63}Cu NMR Evidence for Enhanced Antiferromagnetic Correlations around Zn Impurities in $YBa_2Cu_3O_{6.7}$. *Phys. Rev. Lett.* **2000**, *84* (15), 3422–3425. https://doi.org/10.1103/PhysRevLett.84.3422.

(6) Tarascon, J. M.; Wang, E.; Kivelson, S.; Bagley, B. G.; Hull, G. W.; Ramesh, R. Magnetic versus Nonmagnetic Ion Substitution Effects on Tc in the La-Sr-Cu-O and Nd-Ce-Cu-O Systems. *Phys. Rev. B* **1990**, *42* (1), 218–222. https://doi.org/10.1103/PhysRevB.42.218.

(7) Armitage, N. P.; Fournier, P.; Greene, R. L. Progress and Perspectives on Electron-Doped Cuprates. *Rev. Mod. Phys.* **2010**, *82* (3), 2421–2487. https://doi.org/10.1103/RevModPhys.82.2421.

(8) Tallon, J. L. Normal-State Pseudogap in $Bi_2Sr_2CaCu_2O_8$ Characterized by Impurity Scattering. *Phys. Rev. B* **1998**, *58* (10), R5956–R5959. https://doi.org/10.1103/PhysRevB.58.R5956.

(9) Vom Hedt, B.; Lisseck, W.; Westerholt, K.; Bach, H. Superconductivity in $Bi_2Sr_2CaCu_2O_{8+\delta}$ Single Crystals Doped with Fe, Ni, and Zn. *Phys. Rev. B* **1994**, *49* (14), 9898–9905. https://doi.org/10.1103/PhysRevB.49.9898.

(10) Kuo, Y. K.; Schneider, C. W.; Skove, M. J.; Nevitt, M. V.; Tessema, G. X.; McGee, J. J. Effect of Magnetic and Nonmagnetic Impurities (Ni, Zn) Substitution for Cu in $Bi_2(SrCa)_{2+n}(Cu_{1-x}M_x)_{1+n}O_y$ Whiskers. *Phys. Rev. B* **1997**, *56* (10), 6201–6206. https://doi.org/10.1103/PhysRevB.56.6201.

(11) Guo, Y. F.; Shi, Y. G.; Yu, S.; Belik, A. A.; Matsushita, Y.; Tanaka, M.; Katsuya, Y.; Kobayashi, K.; Nowik, I.; Felner, I.; Awana, V. P. S.; Yamaura, K.; Takayama-Muromachi, E. Large Decrease in the Critical Temperature of Superconducting $LaFeAsO_{0.85}$ Compounds Doped with 3% Atomic Weight of Nonmagnetic Zn Impurities. *Phys. Rev. B* **2010**, *82* (5), 054506. https://doi.org/10.1103/PhysRevB.82.054506.

(12) Li, J.; Guo, Y.; Zhang, S.; Yu, S.; Tsujimoto, Y.; Kontani, H.; Yamaura, K.; Takayama-Muromachi, E. Linear Decrease of Critical Temperature with Increasing Zn Substitution in the

Iron-Based Superconductor $BaFe_{1.89-2x}Zn_{2x}Co_{0.11}As_2$. *Phys. Rev. B* **2011**, *84* (2), 020513. https://doi.org/10.1103/PhysRevB.84.020513.
(13) Li, J.; Guo, Y.-F.; Yang, Z.-R.; Yamaura, K.; Takayama-Muromachi, E.; Wang, H.-B.; Wu, P.-H. Progress in Nonmagnetic Impurity Doping Studies on Fe-Based Superconductors. *Supercond. Sci. Technol.* **2016**, *29* (5), 053001. https://doi.org/10.1088/0953-2048/29/5/053001.
(14) Terashima, K.; Matsui, H.; Hashimoto, D.; Sato, T.; Takahashi, T.; Ding, H.; Yamamoto, T.; Kadowaki, K. Impurity Effects on Electron–Mode Coupling in High-Temperature Superconductors. *Nature Phys* **2006**, *2* (1), 27–31. https://doi.org/10.1038/nphys200.
(15) Drachuck, G.; Salman, Z.; Masters, M. W.; Taufour, V.; Lamichhane, T. N.; Lin, Q.; Straszheim, W. E.; Bud'ko, S. L.; Canfield, P. C. Effect of Nickel Substitution on Magnetism in the Layered van Der Waals Ferromagnet Fe_3GeTe_2. *Phys. Rev. B* **2018**, *98* (14), 144434. https://doi.org/10.1103/PhysRevB.98.144434.
(16) Tian, C.-K.; Wang, C.; Ji, W.; Wang, J.-C.; Xia, T.-L.; Wang, L.; Liu, J.-J.; Zhang, H.-X.; Cheng, P. Domain Wall Pinning and Hard Magnetic Phase in Co-Doped Bulk Single Crystalline Fe_3GeTe_2. *Phys. Rev. B* **2019**, *99* (18), 184428. https://doi.org/10.1103/PhysRevB.99.184428.
(17) May, A. F.; Du, M.-H.; Cooper, V. R.; McGuire, M. A. Tuning Magnetic Order in the van Der Waals Metal Fe_5GeTe_2 by Cobalt Substitution. *Phys. Rev. Materials* **2020**, *4* (7), 074008. https://doi.org/10.1103/PhysRevMaterials.4.074008.
(18) Tian, C.; Pan, F.; Xu, S.; Ai, K.; Xia, T.; Cheng, P. Tunable Magnetic Properties in van Der Waals Crystals $((Fe_{1-x}Co_x)_5GeTe_2$. *Applied Physics Letters* **2020**, *116* (20), 202402. https://doi.org/10.1063/5.0006337.
(19) Ohta, T.; Kurokawa, K.; Jiang, N.; Yamagami, K.; Okada, Y.; Niimi, Y. Enhancement of Spin–Flop-Induced Magnetic Hysteresis in van Der Waals Magnet $(Fe_{1-x}Co_x)_5GeTe_2$. *Applied Physics Letters* **2023**, *122* (15), 152402. https://doi.org/10.1063/5.0141495.
(20) Zhang, H.; Raftrey, D.; Chan, Y.-T.; Shao, Y.-T.; Chen, R.; Chen, X.; Huang, X.; Reichanadter, J. T.; Dong, K.; Susarla, S.; Caretta, L.; Chen, Z.; Yao, J.; Fischer, P.; Neaton, J. B.; Wu, W.; Muller, D. A.; Birgeneau, R. J.; Ramesh, R. Room-Temperature Skyrmion Lattice in a Layered Magnet $(Fe_{0.5}Co_{0.5})_5GeTe_2$. *Sci. Adv.* **2022**, *8* (12), eabm7103. https://doi.org/10.1126/sciadv.abm7103.
(21) Zhu, K.; Wang, M.; Deng, Y.; Tian, M.; Lei, B.; Chen, X. Effect of Co or Ni Substitution on Magnetism in the Layered van Der Waals Ferromagnet Fe_3GaTe_2. *Phys. Rev. B* **2024**, *109* (10), 104402. https://doi.org/10.1103/PhysRevB.109.104402.
(22) Mermin, N. D.; Wagner, H. Absence of Ferromagnetism or Antiferromagnetism in One- or Two-Dimensional Isotropic Heisenberg Models. *Phys. Rev. Lett.* **1966**, *17* (22), 1133–1136. https://doi.org/10.1103/PhysRevLett.17.1133.
(23) Huang, B.; Clark, G.; Navarro-Moratalla, E.; Klein, D. R.; Cheng, R.; Seyler, K. L.; Zhong, D.; Schmidgall, E.; McGuire, M. A.; Cobden, D. H.; Yao, W.; Xiao, D.; Jarillo-Herrero, P.; Xu, X. Layer-Dependent Ferromagnetism in a van Der Waals Crystal down to the Monolayer Limit. *Nature* **2017**, *546* (7657), 270–273. https://doi.org/10.1038/nature22391.
(24) Gong, C.; Li, L.; Li, Z.; Ji, H.; Stern, A.; Xia, Y.; Cao, T.; Bao, W.; Wang, C.; Wang, Y.; Qiu, Z. Q.; Cava, R. J.; Louie, S. G.; Xia, J.; Zhang, X. Discovery of Intrinsic Ferromagnetism in Two-Dimensional van Der Waals Crystals. *Nature* **2017**, *546* (7657), 265–269. https://doi.org/10.1038/nature22060.
(25) Lin, M.-W.; Zhuang, H. L.; Yan, J.; Ward, T. Z.; Puretzky, A. A.; Rouleau, C. M.; Gai, Z.; Liang, L.; Meunier, V.; Sumpter, B. G.; Ganesh, P.; Kent, P. R. C.; Geohegan, D. B.;

Mandrus, D. G.; Xiao, K. Ultrathin Nanosheets of $CrSiTe_3$: A Semiconducting Two-Dimensional Ferromagnetic Material. *J. Mater. Chem. C* **2016**, *4* (2), 315–322. https://doi.org/10.1039/C5TC03463A.

(26) Bonilla, M.; Kolekar, S.; Ma, Y.; Diaz, H. C.; Kalappattil, V.; Das, R.; Eggers, T.; Gutierrez, H. R.; Phan, M.-H.; Batzill, M. Strong Room-Temperature Ferromagnetism in VSe_2 Monolayers on van Der Waals Substrates. *Nature Nanotech* **2018**, *13* (4), 289–293. https://doi.org/10.1038/s41565-018-0063-9.

(27) O'Hara, D. J.; Zhu, T.; Trout, A. H.; Ahmed, A. S.; Luo, Y. K.; Lee, C. H.; Brenner, M. R.; Rajan, S.; Gupta, J. A.; McComb, D. W.; Kawakami, R. K. Room Temperature Intrinsic Ferromagnetism in Epitaxial Manganese Selenide Films in the Monolayer Limit. *Nano Lett.* **2018**, *18* (5), 3125–3131. https://doi.org/10.1021/acs.nanolett.8b00683.

(28) Deng, Y.; Yu, Y.; Song, Y.; Zhang, J.; Wang, N. Z.; Sun, Z.; Yi, Y.; Wu, Y. Z.; Wu, S.; Zhu, J.; Wang, J.; Chen, X. H.; Zhang, Y. Gate-Tunable Room-Temperature Ferromagnetism in Two-Dimensional Fe_3GeTe_2. *Nature* **2018**, *563* (7729), 94–99. https://doi.org/10.1038/s41586-018-0626-9.

(29) Fei, Z.; Huang, B.; Malinowski, P.; Wang, W.; Song, T.; Sanchez, J.; Yao, W.; Xiao, D.; Zhu, X.; May, A. F.; Wu, W.; Cobden, D. H.; Chu, J.-H.; Xu, X. Two-Dimensional Itinerant Ferromagnetism in Atomically Thin Fe_3GeTe_2. *Nature Mater* **2018**, *17* (9), 778–782. https://doi.org/10.1038/s41563-018-0149-7.

(30) Seo, J.; Kim, D. Y.; An, E. S.; Kim, K.; Kim, G.-Y.; Hwang, S.-Y.; Kim, D. W.; Jang, B. G.; Kim, H.; Eom, G.; Seo, S. Y.; Stania, R.; Muntwiler, M.; Lee, J.; Watanabe, K.; Taniguchi, T.; Jo, Y. J.; Lee, J.; Min, B. I.; Jo, M. H.; Yeom, H. W.; Choi, S.-Y.; Shim, J. H.; Kim, J. S. Nearly Room Temperature Ferromagnetism in a Magnetic Metal-Rich van Der Waals Metal. *Sci. Adv.* **2020**, *6* (3), eaay8912. https://doi.org/10.1126/sciadv.aay8912.

(31) May, A. F.; Ovchinnikov, D.; Zheng, Q.; Hermann, R.; Calder, S.; Huang, B.; Fei, Z.; Liu, Y.; Xu, X.; McGuire, M. A. Ferromagnetism Near Room Temperature in the Cleavable van Der Waals Crystal Fe_5GeTe_2. *ACS Nano* **2019**, *13* (4), 4436–4442. https://doi.org/10.1021/acsnano.8b09660.

(32) Wu, Y.; Hu, Y.; Wang, C.; Zhou, X.; Hou, X.; Xia, W.; Zhang, Y.; Wang, J.; Ding, Y.; He, J.; Dong, P.; Bao, S.; Wen, J.; Guo, Y.; Watanabe, K.; Taniguchi, T.; Ji, W.; Wang, Z.; Li, J. Fe-Intercalation Dominated Ferromagnetism of van Der Waals Fe_3GeTe_2. *Advanced Materials* **2023**, *35* (36), 2302568. https://doi.org/10.1002/adma.202302568.

(33) May, A. F.; Bridges, C. A.; McGuire, M. A. Physical Properties and Thermal Stability of $Fe_{5-x}GeTe_2$ Single Crystals. *Phys. Rev. Materials* **2019**, *3* (10), 104401. https://doi.org/10.1103/PhysRevMaterials.3.104401.

(34) Li, Z.; Guo, D.; Huang, K.; Ma, G.; Liu, X.; Wu, Y.; Yuan, J.; Tao, Z.; Wang, B.; Wang, X.; Zou, Z.; Yu, N.; Yu, G.; Xue, J.; Liu, Z.; Ji, W.; Li, J.; Guo, Y. Robust Weak Antilocalization Effect Up to ∼120 K in the van Der Waals Crystal $Fe_{5-x}GeTe_2$ with Near-Room-Temperature Ferromagnetism. *J. Phys. Chem. Lett.* **2023**, *14* (23), 5456–5465. https://doi.org/10.1021/acs.jpclett.3c00380.

(35) Oliveira, F. M.; Antonatos, N.; Mazánek, V.; Sedmidubský, D.; Sofer, Z.; Gusmão, R. Exfoliated Fe_3GeTe_2 and Ni_3GeTe_2 Materials as Water Splitting Electrocatalysts. *FlatChem* **2022**, *32*, 100334. https://doi.org/10.1016/j.flatc.2022.100334.

(36) Papavasileiou, A. V.; Menelaou, M.; Sarkar, K. J.; Sofer, Z.; Polavarapu, L.; Mourdikoudis, S. Ferromagnetic Elements in Two-Dimensional Materials: 2D Magnets and Beyond. *Adv Funct Materials* **2024**, *34* (2), 2309046. https://doi.org/10.1002/adfm.202309046.

(37) Chen, X.; Shao, Y.-T.; Chen, R.; Susarla, S.; Hogan, T.; He, Y.; Zhang, H.; Wang, S.; Yao, J.; Ercius, P.; Muller, D. A.; Ramesh, R.; Birgeneau, R. J. Pervasive beyond Room-Temperature Ferromagnetism in a Doped van Der Waals Magnet. *Phys. Rev. Lett.* **2022**, *128* (21), 217203. https://doi.org/10.1103/PhysRevLett.128.217203.
(38) Zhang, G.; Guo, F.; Wu, H.; Wen, X.; Yang, L.; Jin, W.; Zhang, W.; Chang, H. Above-Room-Temperature Strong Intrinsic Ferromagnetism in 2D van Der Waals Fe_3GaTe_2 with Large Perpendicular Magnetic Anisotropy. *Nat Commun* **2022**, *13* (1), 5067. https://doi.org/10.1038/s41467-022-32605-5.
(39) Li, Z.; Zhang, H.; Li, G.; Guo, J.; Wang, Q.; Deng, Y.; Hu, Y.; Hu, X.; Liu, C.; Qin, M.; Shen, X.; Yu, R.; Gao, X.; Liao, Z.; Liu, J.; Hou, Z.; Zhu, Y.; Fu, X. Room-Temperature Sub-100 Nm Néel-Type Skyrmions in Non-Stoichiometric van Der Waals Ferromagnet $Fe_{3-x}GaTe_2$ with Ultrafast Laser Writability. *Nat Commun* **2024**, *15* (1), 1017. https://doi.org/10.1038/s41467-024-45310-2.
(40) Hou, X.; Wang, H.; Zhang, B.; Xu, C.; Sun, L.; Li, Z.; Wang, X.; Qu, K.; Wei, Y.; Guo, Y. Room-Temperature Skyrmions in the van Der Waals Ferromagnet Fe_3GaTe_2. *Applied Physics Letters* **2024**, *124* (14), 142404. https://doi.org/10.1063/5.0204185.
(41) Deiseroth, H.; Aleksandrov, K.; Reiner, C.; Kienle, L.; Kremer, R. K. Fe_3GeTe_2 and Ni_3GeTe_2 – Two New Layered Transition-Metal Compounds: Crystal Structures, HRTEM Investigations, and Magnetic and Electrical Properties. *Eur J Inorg Chem* **2006**, *2006* (8), 1561–1567. https://doi.org/10.1002/ejic.200501020.
(42) Li, X.; Zhu, M.; Wang, Y.; Zheng, F.; Dong, J.; Zhou, Y.; You, L.; Zhang, J. Tremendous Tunneling Magnetoresistance Effects Based on van Der Waals Room-Temperature Ferromagnet Fe_3GaTe_2 with Highly Spin-Polarized Fermi Surfaces. *Applied Physics Letters* **2023**, *122* (8), 082404. https://doi.org/10.1063/5.0136180.
(43) Lee, J.-E.; Yan, S.; Oh, S.; Hwang, J.; Denlinger, J. D.; Hwang, C.; Lei, H.; Mo, S.-K.; Park, S. Y.; Ryu, H. Electronic Structure of Above-Room-Temperature van Der Waals Ferromagnet Fe_3GaTe_2. *Nano Lett.* **2023**, *23* (24), 11526–11532. https://doi.org/10.1021/acs.nanolett.3c03203.
(44) Ruiz, A. M.; Esteras, D. L.; López-Alcalá, D.; Baldoví, J. J. On the Origin of the Above-Room-Temperature Magnetism in the 2D van Der Waals Ferromagnet Fe_3GaTe_2. *Nano Lett.* **2024**, *24* (26), 7886–7894. https://doi.org/10.1021/acs.nanolett.4c01019.
(45) Yang, H.-H.; Bansal, N.; Rüßmann, P.; Hoffmann, M.; Zhang, L.; Go, D.; Li, Q.; Haghighirad, A.-A.; Sen, K.; Blügel, S.; Le Tacon, M.; Mokrousov, Y.; Wulfhekel, W. Magnetic Domain Walls of the van Der Waals Material Fe_3GeTe_2. *2D Mater.* **2022**, *9* (2), 025022. https://doi.org/10.1088/2053-1583/ac5d0e.

ASSOCIATED CONTENT

Supporting Information

The Supplementary Information (PDF) is available free of charge at https://pubs.acs.org.

Results of the Powder X-ray Diffraction (PWXRD) and the energy-dispersive X-ray spectrum (EDS) measurements of bulk $(Fe_{1-x}Ni_x)_3GaTe_2$ crystals, LTEM and MOKE results of $(Fe_{1-x}Ni_x)_3GaTe_2$ samples.

AUTHOR INFORMATION

Corresponding Authors

Shihao Zhang – *School of Physics and Electronics, Hunan University, Changsha 410082, China*

Email: zhangshh@hnu.edu.cn

Xuewen Fu –*Ultrafast Electron Microscopy Laboratory, Key Laboratory of Weak-Light Nonlinear Photonics (Ministry of Education), School of Physics, Nankai University, Tianjin 300071, China*

Email: xwfu@nankai.edu.cn

Ke Qu –*School of Physics and Electronic Science, East China Normal University, Shanghai 200241 China*

Email: kqu@chem.ecnu.edu.cn

Yanfeng Guo – *School of Physical Science and Technology, ShanghaiTech University, Shanghai 201210, China; ShanghaiTech Laboratory for Topological Physics, Shanghai 201210, China;*

Email: guoyf@shanghaitech.edu.cn

Authors

Jian Yuan – *School of Physical Science and Technology, ShanghaiTech University, Shanghai 201210, China*

Haonan Wang – *School of Physics and Electronic Science, East China Normal University, Shanghai 200241 China*

Xiaofei Hou – *School of Physical Science and Technology, ShanghaiTech University, Shanghai 201210, China*

Binshuo Zhang – *School of Physical Science and Technology, ShanghaiTech University, Shanghai 201210, China*

Yurui Wei – *School of Information Science and Technology, ShanghaiTech University, Shanghai 201210, China*

Jiangteng Guo – *Ultrafast Electron Microscopy Laboratory, Key Laboratory of Weak-Light Nonlinear Photonics (Ministry of Education), School of Physics, Nankai University, Tianjin 300071, China*

Lu Sun – *School of Information Science and Technology, ShanghaiTech University, Shanghai 201210, China*

Zhenhai Yu – *School of Physical Science and Technology, ShanghaiTech University, Shanghai 201210, China*

Zhikai Li – *School of Physical Science and Technology, ShanghaiTech University, Shanghai 201210, China*

Xiangqi Liu – *School of Physical Science and Technology, ShanghaiTech University, Shanghai 201210, China*

Wei Xia – *School of Physical Science and Technology, ShanghaiTech University, Shanghai 201210, China*

Xia Wang – *School of Physical Science and Technology, ShanghaiTech University, Shanghai 201210, China*; *Analytical Instrumentation Center, School of Physical Science and Technology, ShanghaiTech University, Shanghai 201210, China*

Xuerong Liu – *School of Physical Science and Technology, ShanghaiTech University, Shanghai 201210, China*

Yulin Chen – *School of Physical Science and Technology, ShanghaiTech University, Shanghai 201210, China; Clarendon Laboratory, Department of Physics, University of Oxford, Oxford OX1 3PU, United Kingdom*

Zhenzhong Yang – *Key Laboratory of Polar Materials and Devices (MOE), Ministry of Education, Shanghai Center of Brain-inspired Intelligent Materials and Devices, Department of Electronics, East China Normal University, Shanghai 200241, China*

Acknowledgments

The authors acknowledge the National Key R&D Program of China (Grants No. 2023YFA1406100), the Shanghai Science and Technology Innovation Action Plan (Grant No. 21JC1402000) and the National Nature Science Foundation of China (Grant No. 920651, 11934017). Y.F.G. acknowledges the open research fund of Beijing National Laboratory for Condensed Matter Physics (2023BNLCMPKF002). S.H.Z. was supported by the National Natural Science Foundation of China (12304217) and the Fundamental Research Funds for the Central Universities from China. The authors also thank the support from Analytical Instrumentation Center (#SPST-AIC10112914) and the Double First-Class Initiative Fund of ShanghaiTech University.

Author contributions

Y.F.G. conceived the project. J.Y. synthesized the single crystals and carried out structural characterizations, measured the magnetotransport properties and analyzed the data with the help from X.F.H., B.S.Z., Z.H.Y., Z.K.L., X.Q.L., W.X., X.W. and X.R.L. J.T.G. and X.W.F. measured and analyzed the Lorentz TEM data. S.H.Z. performed the first-principles calculations. H.N.W, K.Q and Z.Z.Y. measured the atomic-resolution crystal structure by using STEM. Y.L.C. provided very useful discussions. †J.Y., H.N.W., X.F.H. and B.S.Z. contributed equally to this work. Y.F.G. wrote the manuscript with input from all authors.

Competing interests

The authors declare no competing interest.

Data Availability

The data that support the findings of this study are available from the corresponding authors upon reasonable request.

Additional Information

Correspondence and requests for materials should be addressed to Y.F.G. (guoyf@shanghaitech.edu.cn), Ke Qu (kqu@chem.ecnu.edu.cn), Xuewen Fu (xwfu@nankai.edu.cn) or Shihao Zhang (zhangshh@hnu.edu.cn)

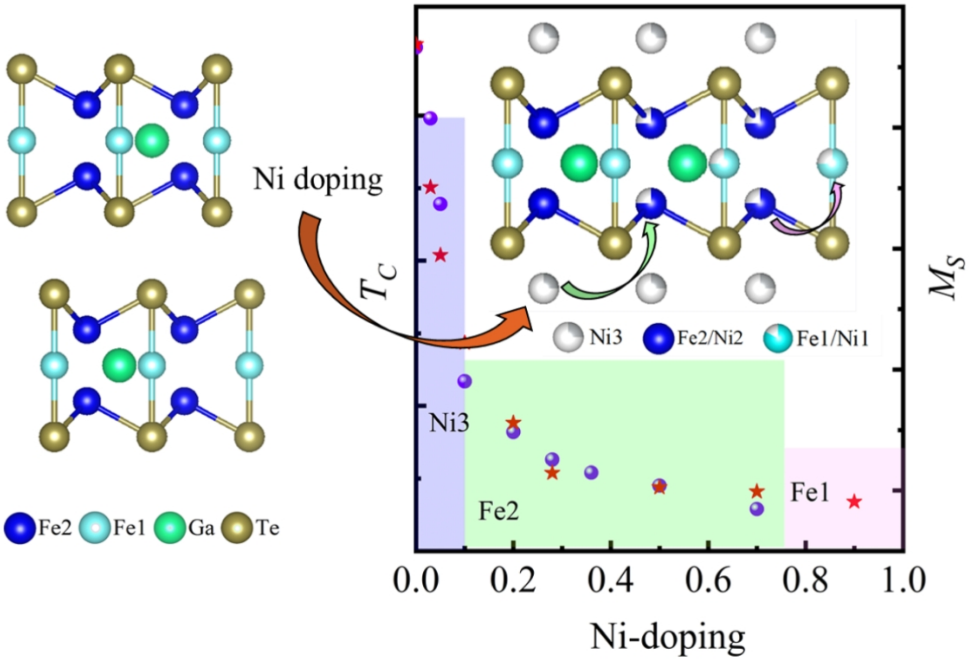

Three-step Ni substitution for Fe in (Fe1-xNix)3GaTe2, resulting in nonlinear decrease of both the Curie temperature TC and saturation magnetic moments MS, which is tightly tied to the Ni occupancy order as well as the different roles of Ni3, Fe1 and Fe2 sites in the spin Hamiltonian.

55x50mm (600 x 600 DPI)